Friction

Research Article

Development of a new procedure to determine the different wear stages on ball-on-disc test

Ester Villanueva[1,✉], Iban Vicario[1], Raúl Cosgaya[2], Teresa Guraya[2], Iñaki Hurtado[3], Joseba Albizuri[2]

Cite this article: Villanueva E, Vicario I, Cosgaya R, et al. *Friction* 2026, **14**: 9441227. https://doi.org/10.26599/FRICT.2026.9441227

ABSTRACT: This study proposes a numerical methodology based on the application of first-, second-, and third-order derivatives to analyse the evolution of the coefficient of friction (CoF) obtained from ball-on-disc (BoD) wear tests. The approach aims to provide an objective and quantitative identification of mechanisms, wear stages, and transition points, overcoming the subjectivity commonly associated with conventional friction curve interpretation. Before derivative computation, the CoF signal was smoothed to reduce experimental noise while preserving the morphological features of the friction curve. The methodology was applied to a newly developed multicomponent Al80Mg10Si5Cu5 high-pressure die casting (HPDC) alloy tested under dry sliding at room temperature (RT). The derivative-based analysis enabled the identification of successive wear stages, from the initial settling and running-in to transient and quasi-stationary regimes, and the determination of characteristic transition points, correlated with wear mechanisms through surface and microstructural analyses. The results demonstrate that the proposed methodology enables an objective determination of the duration and sequence of wear stages, reveals that the transition to stable sliding does not coincide with the maximum CoF value, and improves the identification of highly dynamic early wear regimes that are often underestimated by visual analysis. Due to its low computational cost and reliance on signals commonly available in tribological systems, the proposed derivative-based methodology shows strong potential for real-time friction and wear monitoring, predictive maintenance, and the automation of tribological control systems, although further validation under industrial operating conditions is required.

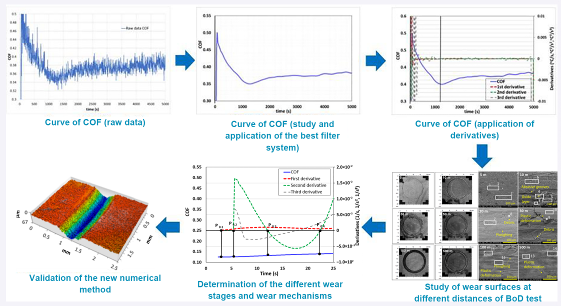

KEYWORDS: friction; wear; ball-on-disc; derivatives; multicomponent aluminium alloy; high-pressure die casting

1 Introduction

Friction losses significantly affect the performance and reliability of mechanical components. In many automotive components, materials are specifically designed to provide controlled frictional behaviour. In this context, the fundamentals of tribology have been extensively studied in the literature [1–3].

The ball-on-disc (BoD) test has been widely adopted to investigate friction and wear processes under sliding conditions. It is thoroughly documented [4], with a pin or spherical counterbody pressed against a rotating disc under a controlled normal load and sliding velocity [5–7], under lubricated or dry sliding conditions [8, 9]. During the BoD test, the evolution of the coefficient of friction (CoF) is continuously recorded as a function of time or sliding distance. In most studies, the analysis of the CoF curve is limited to the identification of a running-in period followed by a steady-state regime, often based on averaged values or qualitative visual inspection [10]. Although several studies have reported that friction curves exhibit multiple stages or regimes [11–13], stage boundaries are frequently defined using descriptive interpretations or the maximum CoF value, without explicit quantitative criteria capable of capturing intermediate transitions. Measurement noise, signal oscillations, and the coexistence of multiple wear mechanisms further complicate the accurate interpretation of stage onset and duration [14], leading to subjective or inconsistent interpretations [15, 16].

Some approaches apply signal smoothing or numerical tools to visually delimit different regimes [17]; while others relate the area under the CoF curve to wear behaviour, indicating that the steady-state CoF alone is not always a reliable indicator of total wear rate [18]. However, a robust and quantitative framework for objectively identifying wear stages and mechanisms remains lacking, with a need for advanced signal analysis techniques to extract the dynamic information [19].

Aluminium alloys exhibit complex wear behaviour governed by multiple mechanisms, including abrasion, adhesion, plastic deformation, delamination, and tribochemical effects [20].

[1] TECNALIA, Basque Research and Technology Alliance (BRTA), Astondo Bidea, 700, Derio, Bizkaia, Spain. [2] Faculty of Engineering of Bilbao, University of the Basque Country (UPV/EHU), Bilbao E48013, Spain. [3] Mechanical and Manufacturing Department, Mondragon University, Arrasate-Mondragon E20500, Spain.

✉ Corresponding author. E-mail: ester.villanueva@tecnalia.com

Received: September 3, 2025; Revised: January 26, 2026; Accepted: January 27, 2026

Common wear modes involve abrasive cutting and ploughing, material transfer, and plastic delamination [21, 22], which strongly depend on contact conditions, temperature, and microstructure [13, 23, 24].

Surface roughness strongly influences contact mechanics, friction evolution, and wear mechanisms [25]; but its accurate characterisation and correlation with functional performance remain open challenges [26]. In high-pressure die casting (HPDC), the presence of a surface skin with refined microstructure and reduced defects further modifies the initial contact conditions of the test, and surface skin affects the early stages of sliding, delaying full metallic contact and altering wear evolution [27, 28].

Advanced statistical and computational techniques are increasingly required to extract meaningful information from complex experimental signals [29]. Derivative-based approaches are well established in other fields, where higher-order derivatives of temperature–time curves are used to identify characteristic transformation points and low-energy events [30–35]. Despite their application in other fields, their systematic application to the interpretation of friction curves remains limited [19]. In this context, the present work proposes a derivative-based methodology using the first (1st), second (2nd), and third (3rd) derivatives of the COF curve to enable an objective and quantitative analysis of friction evolution. Before derivative computation, a signal filtering procedure was applied to reduce noise while preserving the morphological features of the friction curve. The proposed approach allowed the precise identification of wear stages and transition points, providing an accurate determination of the onset and termination of each stage and their correlation with dominant wear mechanisms. In particular, the steady stage was shown not to coincide with the maximum CoF value but to occur subsequently at a characteristic low-energy transition point in the friction curve.

The methodology was applied to an Al80Mg10Si5Cu5 aluminium alloy produced by HPDC, designed for high wear resistance [36, 37]. Validation was achieved by correlating derivative-based indicators with wear evolution and surface topography. Overall, this approach provides a robust quantitative tool for understanding friction and wear behaviour, with strong potential for monitoring and anticipating changes in wear mechanisms and for supporting the automation of wear control systems.

2 Methodology

2.1 Signal filtering

First, to mitigate experimental noise and micro-fluctuations in the CoF curve that may distort derivative calculations and produce false stage transitions, the raw data were grouped and smoothed [38, 39]. Several types of filters (Chebyshev type I and type II, FIR, Cauer, Savitzky–Golay, Butterworth, Bessel, Gaussian, moving average, and median) were studied, according to their function and possible implementation [40]. The filtering process was performed using Python software, version 3.12 (2023). To apply the filtering systems, the data from the minimum ΔT was interpolated, ensuring a uniform sampling [41]. Some filters over-smoothed the signal and may suppress relevant events (inflection points), whereas others either failed to sufficiently attenuate noise or introduced signal displacement (phase shifts), resulting in unstable derivative response. The centred moving average filter was selected because it smooths the signal by averaging data points within a sliding window, whose time duration determines its effective bandwidth. The number of points included in the averaging window depends on the sampling frequency. It is very suitable for smoothing applications characterized by a flat response at low frequencies, smooth transitions, and effective attenuation of high-frequency fluctuations [42], providing a stable basis for derivative computation without requiring additional assumptions. Some previous studies have applied it to friction signal analysis, supporting the suitability and reproducibility of the chosen approach [19].

The centred moving average filter is defined by Eq. (1):

$$y[n] = \frac{1}{2M+1}\sum_{k=-M}^{M} x[n+k] \tag{1}$$

where $x[n]$ represents the original discrete signal, $y[n]$ the filtered signal, n the sample index, $x[n+k]$ the values of the original signal within a window of length $2M + 1$ centred at n, and M the number of samples taken on either side of the central value, with $M = 30$.

2.2 Proposed analysis method

The CoF smoothed signal can be treated as a continuous time-dependent signal suitable for numerical differentiation. While the filtered CoF curve provides a clearer representation of the global frictional behaviour, subtle changes associated with transitions between wear regimes or low-energy tribological events may remain hidden. To extract this information, a derivative-based analytical approach is proposed, in which the smoothed CoF curve and its successive derivatives were analysed as a function of time. The 1st derivative (d(CoF)/dt) represents the rate of change of friction [43] and is related to the onset, intensity, and direction of transitions between wear regimes. The 2nd derivative (d^2(CoF)/dt^2) describes the acceleration, deceleration, or the rate of change of the velocity at which it moves and provides information on the initiation or termination of tribological events, with its zero-crossings corresponding to turning points in the CoF evolution. The 3rd derivative (d^3(CoF)/dt^3), commonly referred to as jerk, is particularly sensitive to rapid variations in acceleration and micro-instabilities in the frictional response, with near-zero values indicating stable sliding conditions [32, 33]. The first and successive derivatives can be calculated using a standard differential quotient derivative algorithm, in which the derivative for each data point is calculated by averaging the differential quotients between two adjacent data points and the data point of interest [44]. In Fig. 1, the mentioned algorithm is graphically represented and calculated using Eqs. (2) and (3).

The slopes S_{21} between points P_2 and P_1 and S_{32} between the data points P_3 and P_2 follow Eq. (2):

$$S_{21} = \frac{\partial y_{21}}{\partial x_{21}} = \frac{y_2 - y_1}{x_2 - x_1} \text{ and } S_{32} = \frac{\partial y_{32}}{\partial x_{32}} = \frac{y_3 - y_2}{x_3 - x_2} \tag{2}$$

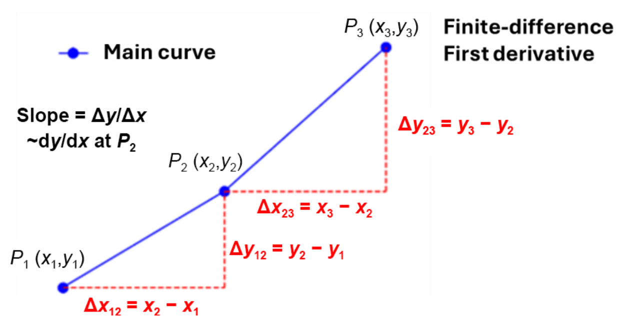

Fig. 1 Finite-difference scheme used to estimate the first derivative from discrete data.

The derivative D_2 of data point P2 is calculated by means of Eq. (3):

$$D_2 = \frac{S_{21} + S_{32}}{2} \tag{3}$$

3 Experimental procedure

3.1 Materials and manufacturing processes

The Al80Mg10Si5Cu5 alloy was manufactured by HPDC, with a 950 t injection machine (PT-650, Pretansa). A 500 kg capacity electrical furnace (Dugo EBC, Dugopa) was employed for melting and holding the alloy. As charge material, returns and ingots of AlSi7Mg, AM60B, and AlSi9Cu3 alloys were employed, acting as the melting bath base. The working temperature was adjusted to 700 °C, and the molten metal was injected at 680 °C. Casting parts were extracted and immersed in water at 50 °C.

3.2 Analysis of chemical composition

The composition of the experimental alloy was determined before and after the casting process by a discharge optical emission spectrometer (OES; Spectro, Spectrolab).

3.3 Ball-on-disc wear test

Dry sliding wear friction tests were carried out in a sphere-on-plate reciprocating configuration using a tribometer with BoD mode. The tests were performed at RT according to the ASTM G99-05 [45]. Figure 2 displays the equipment and procedure. Alumina balls with a 6 mm diameter and a hardness of 1,250–1,700 HV were used as counter-face bodies. Test conditions are summarized in Table 1. The data acquisition of CoF during the test was performed using MT4002 software (version 12.0, Microtest S.A.), connected to a BoD tribometer (MT2/60/NI, Microtest S.A.), which provides a friction force resolution of ±0.2 mN. The repeatability was ensured by repeating the test at least three times. Plate-shaped casting test plates were machined into test coupons of about 50 mm × 50 mm × 5 mm.

3.4 Determination of the wear rate

The specific wear rate was evaluated using a three-dimensional (3D) laser scanning confocal microscope (DCM 3D, Leica), providing an accurate measurement of the real geometry of the wear track, with high-resolution topographical information [46, 47]. The total wear area was determined by analysing at least 16 two-dimensional (2D) sectional profiles uniformly distributed along the wear track using Leica map software. For each profile, a line scan perpendicular to the sliding direction was extracted, and the enclosed area was calculated. The wear volume was then obtained by multiplying the average cross-sectional area by the circumference of the wear track, and the specific wear rate was calculated in terms of volume loss per unit load and sliding distance ($mm^3/(N·m)$) by dividing the total worn volume by the applied normal load and the total sliding distance [48, 49]. In addition, the worn surface and subsurface regions were systematically examined to identify the prevailing wear mechanisms and damage features. Microstructural and compositional analyses were carried out using a scanning electron microscope (SEM) coupled with an energy-dispersive X-ray spectrometer (EDS) (ESEM; Quanta 200, FEI).

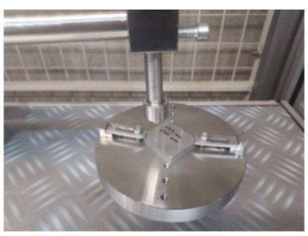

Fig. 2 Detail of sample mounted on tribometer arm.

Table 1 BoD test parameters

Test parameter	Selected value
Load (N)	15
Velocity (m/s)	0.1
Rotation speed (r/min)	127.33
Sliding distance (m)	500
Track diameter (mm)	15
Environment	Dry air
Relatively humidity	40%

4 Results and discussion

4.1 Chemical composition of the experimental alloys

Table 2 summarizes the chemical composition of the Al80Mg10Si5Cu5 HPDC alloy.

4.2 Analysis of ball-on-disc test and application of signal filtering

Figure 3 shows the raw and smoothed CoF curves. The raw CoF signal exhibited pronounced fluctuations and a high dispersion, particularly at elevated CoF values, whereas the smoothed curve preserved the overall trend, retaining the critical features of the friction curve without any noticeable phase delay. The different wear stages, identified based on friction data [11–13], were also highlighted. While these stages could be visually estimated from the smoothed curve, their identification became more challenging when using the raw, unsmoothed signal.

Low CoF values, approximately 0.1, were first measured, and then, CoF values increased, reaching a maximum of about 0.50. At around 20 m (200 s), CoF values decreased until a steady value of

Table 2 Chemical composition (wt%) of Al80Mg10Si5Cu5 HPDC alloy

Reference	Al	Si	Fe	Cu	Mn	Mg	Zn
Al80Mg10Si5Cu5	78.93	5.63	0.25	4.67	0.13	10.32	0.08

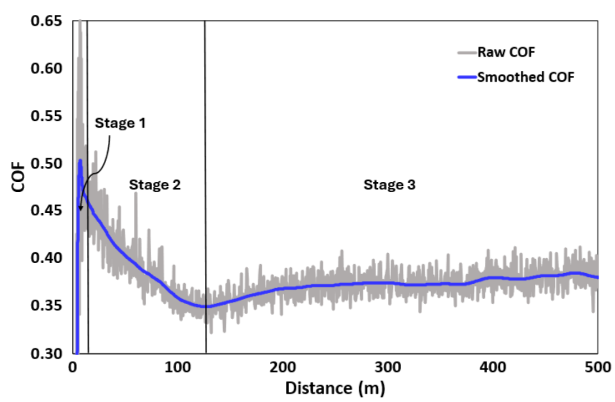

Fig. 3 CoF recorded values (raw and smoothed) for as-cast Al80Mg10Si5Cu5 HPDC alloy.

清華大学出版社 Tsinghua University Press | SciOpen

approximately 0.375 was reached at around 100 m (1,000 s), after which the values remained stable or showed a slight increasing trend.

Table 3 summarizes the mean values and standard deviations (μ) obtained from both raw and smoothed friction curves, and the specific wear rate (K), all of which should be interpreted as comparative indicators for the Al80Mg10Si5Cu5/alumina friction pair under the specific experimental conditions of this study.

In Fig. 4, we can observe many possible points that could be defined as the starting or end of the different stages directly from the original smoothed curve, yet it is not clear from the raw curve.

4.3 Study of topography at different distances

Wear rate was obtained at periodic interruptions, as shown in Fig. 5. There was a progressive increase in track width and height with distance up to the total sliding distance of 500 m, with material removal faster in the first stages, and then, a steady-state condition was reached at around 100 m and maintained until the end of the test..

Table 3 COF and wear rate coefficient values of Al80Mg10Si5Cu5 HPDC

Curve COF	μ	K (mm³/(N·m))
Raw curve	0.38±0.01	(9.9±1.9)×10⁻⁴
Smoothed curve	0.38±0.008	

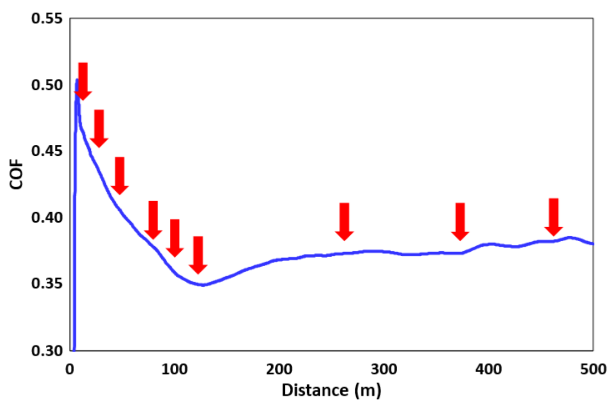

Fig. 4 Friction curve indicating possible characteristic regions by SEM and optical profilometry.

In the first 5 m, the wear track was very smooth, with some material loss, and the wear track became clearly visible after approximately 10 m. After 30 m, debris material was observed on the worn track. These findings agree with the results obtained in Fig. 6. They provide evidence of a significant material removal in the range of 5–100 m, and then, the wear rate decreased progressively with increasing distance, as an asymptotic curve.

The different wearing mechanisms and friction behaviour were studied by analysing the morphology and chemical composition of the worn area at different distances using SEM and EDS, as shown in Fig. 7.

During the first 5 m, the sample surface appeared quite smooth, with only some removed material along the sliding direction. Corresponding EDS analyses revealed the absence of an oxide layer in the worn surface (points 1 and 2 in Table 4), showing a very similar composition to the matrix composition.

After 10 m, small debris oxide particles (point 3) and some plastic deformed areas (points 4 and 5) were detected as a consequence of the plastic deformation of the material asperities [14, 49]. Because of the dragging of some debris embedded in the aluminium matrix, abrasive grooves running along the sliding direction began to be created, leading to an abrasion wear mechanism. These oxides were not uniformly presented on the worn track as observed in various areas (point 6).

At 20 m, the formation of more uniform debris was observed (points 7 and 8). Also, plough lines were visible above the wear track, confirming that abrasion is the main wear mechanism.

After 30 m, more pronounced ploughing was detected, with some oxide particles (point 9) which can be compacted on the surface and prevent adhesive wear [50]. While larger phases are generally detached from the track, coarse phases remain embedded in the matrix, with the hard oxide particles being responsible for micro-cutting the surface and causing the plastic

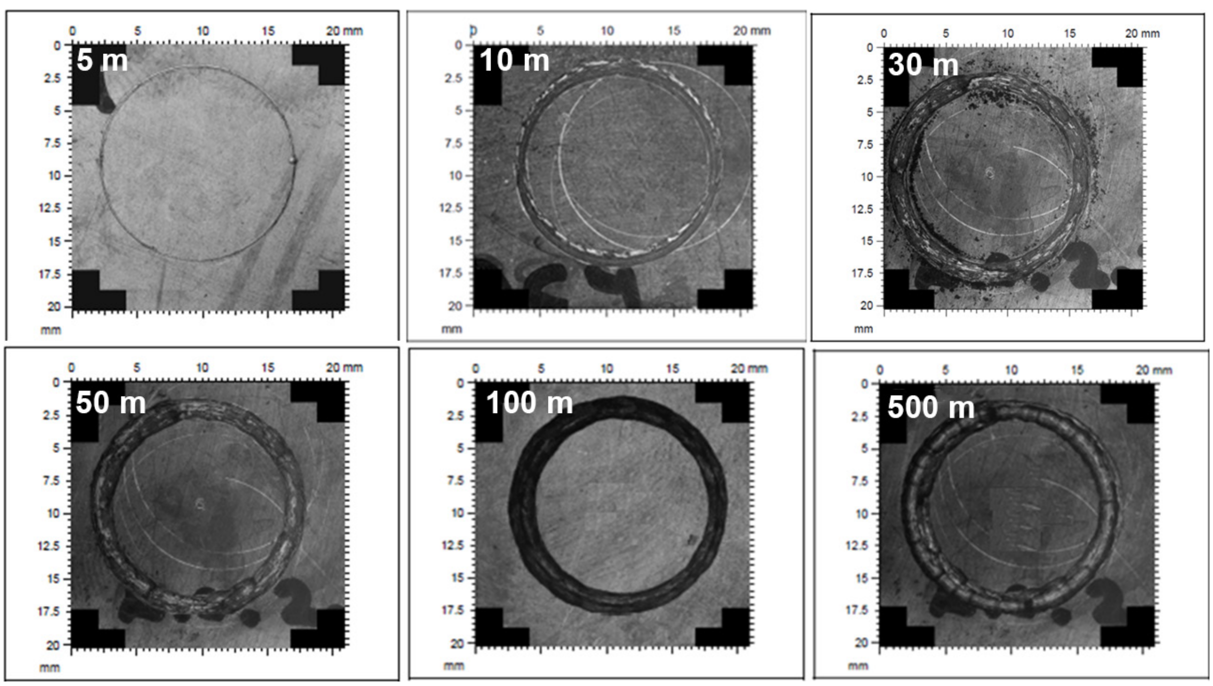

Fig. 5 3D projections of samples at different test distances.

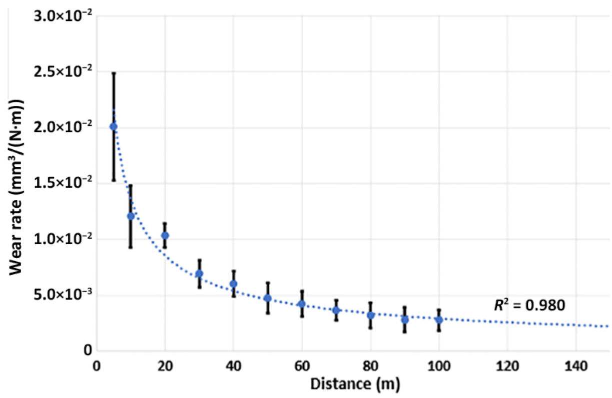

Fig. 6 Wear rate evolution with test distance.

deformation of the matrix. Therefore, plastic deformation of the worn area on the exterior diameter of the track was visible.

Finally, between 100 and 500 m, abrasion was characterized by regions with surface grooves and some parallel ploughing produced by abrasive fragments, as shown in point 11. This debris on the wear track can result in a slight increase in the friction values [14].

Subsequently, the chemical compositions of the above-mentioned points examined by EDS are collected in Table 4.

4.4 Use of the derivative-based methodology on the friction curve

In this section, each stage and the characteristic points determined by derivatives are described.

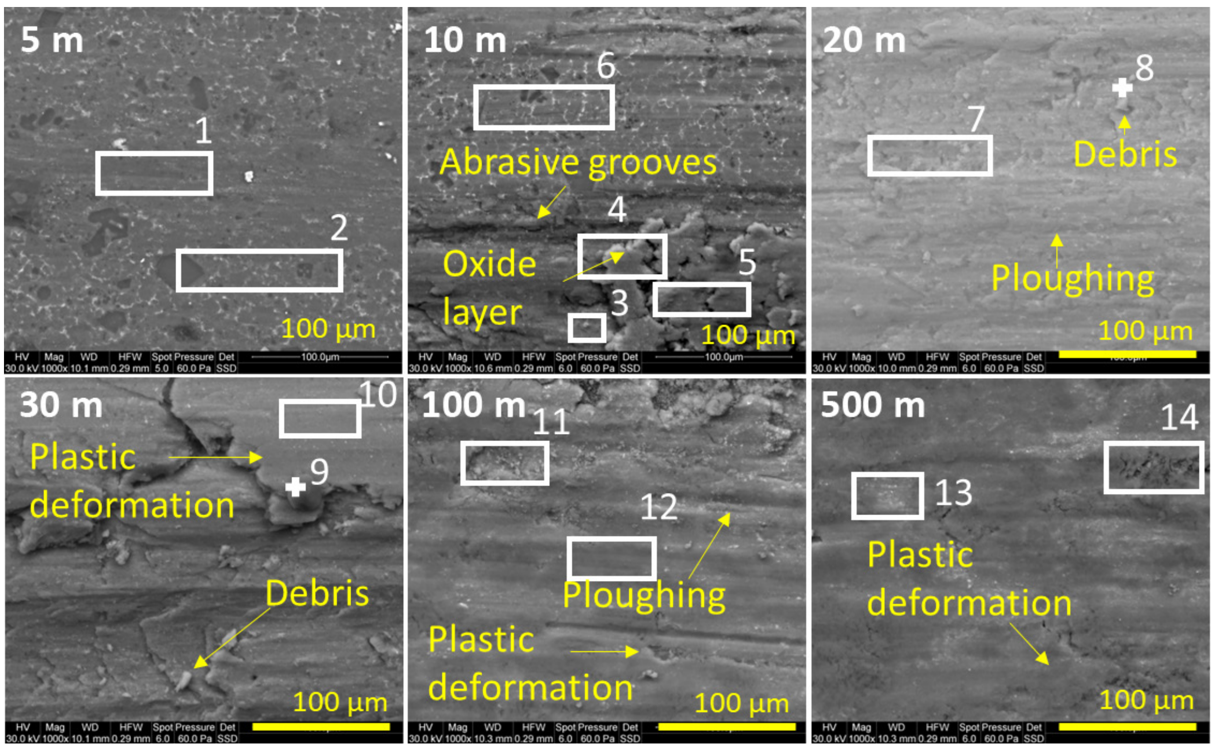

Fig. 7 SEM and EDS analysis at different test distances.

Table 4 EDS composition (wt%) of the analyzed points

Area/point	O	Al	Mg	Si	Cu	Fe
1	—	81.3	10.0	4.3	4.3	—
2	—	82.0	9.7	4.1	4.2	—
3	1.3	77.8	9.3	1.4	10.2	—
4	4.5	73.2	13.0	5.1	4.0	0.3
5	4.5	75.8	11.5	3.4	4.8	—
6	4.1	80.8	7.8	2.8	4.5	—
7	2.3	69.7	16.1	9.0	2.9	—
8	3.8	66.4	17.8	9.0	2.8	—
9	15.0	20.2	3.4	59.7	1.7	—
10	2.0	78.3	10.7	4.2	4.9	—
11	27.8	56.5	9.0	3.0	3.7	—
12	27.7	56.8	9.1	2.8	3.7	—
13	11.5	68.2	9.2	2.9	7.6	0.6
14	27.1	55.8	7.8	2.6	6.7	—

4.4.1 Previous phase or zero phase

The previous stage is related to the settling of materials in the test bar. Also, the first fracture and deformation of the softer surface asperities can take place [51]. Using the derivative method, four characteristic points were defined to describe the zero phase, as shown in Fig. 8.

The first characteristic point corresponds to the starting point $P_{0.1}$, where the velocity (1st derivative) and acceleration (2nd derivative) begin to increase. It is identified by the positive zero crossing of the 1st and 2nd derivatives. At this stage, the ball starts to move over the sample surface, although friction remains negligible.

In $P_{0.2}$, the acceleration reaches an initial maximum within this stage, while the velocity remains positive, as identified by the negative zero crossing of the 3rd derivative. CoF begins to increase slightly, and the velocity continues to rise, but at a reduced rate, associated with the first punctual contacts between the ball and surface asperities, leading to local abrasion and a temporary deceleration of the motion, which contributes to the initial increase in CoF [11, 52].

At $P_{0.3}$, the velocity reaches its maximum value within this initial stage, while the acceleration becomes negative, as identified by the negative zero crossing of the 2nd derivative. After this point, the velocity gradually decreases, and a slight reduction in the frequency of oscillations is observed, which can be related to the progressive removal of surface asperities [52] and the generation of fine wear debris [53], which promotes a more conformal contact between the sliding surfaces.

Point $P_{0.4}$ marks the end of this preliminary stage and coincides with the beginning of stage 1 ($P_{1.1}$). At this point, both velocity and acceleration return to positive values, as identified by the positive zero crossing of the 2nd derivative, reflecting an increase in the relative motion between the ball and the surface, while the CoF remains nearly constant and very low, indicating that full frictional engagement has not yet been established.

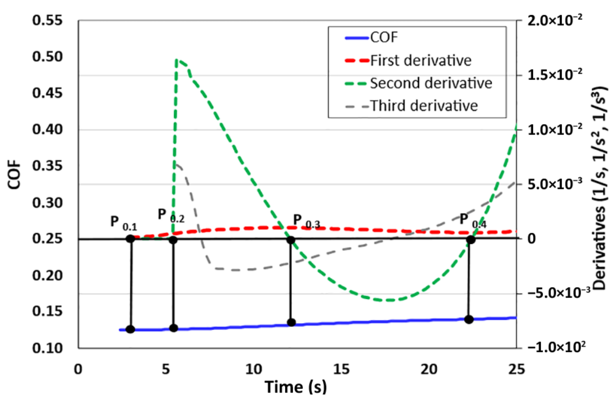

Fig. 8 Detail of previous stage determination applying derivatives.

In Fig. 9, 2D and 3D optical surface profilometry analyses at 5 m are shown, with a slight penetration of the ball in the sample (up to about 67 μm) and the suppression of surface asperities.

The analysed area at 5 m (50 s) is very close to that at 2.5 m (25 s), demonstrating that derivative-based analysis can define the settling of the materials and identify the stage 0 zone, as the settlement has been performed.

4.4.2 Stage 1

In this stage, the CoF values start to increase until the shear strength of the junctions is reached [54], presenting high magnitude values of velocity and acceleration. Although stage 1 corresponds to a single physical running-in regime, the derivative-based analysis reveals several internal transition points associated with changes in dominant contact and wear mechanisms. Up to twelve characteristic points describing this stage can be observed, as described in Fig. 10.

$P_{1.1}$ marks the beginning of stage 1, with velocity and acceleration curves starting to present positive values, determined by the positive zero crossing of the 1st and 2nd derivatives with respect to the *x*-axis. Also, the 3rd derivative or super-acceleration curve starts to become visible. An increased movement between the ball and the surface is presented, but there is nearly no friction, with the CoF remaining constant. This has coincided with the moment when the amount of debris on the track is equal to that leaving the contact surface [55].

In $P_{1.2}$, the super-acceleration curve reaches its maximum value. From this point onward, CoF values start to increase due to friction, increasing the acceleration. With super-acceleration, abrupt and sharp movements take place [56], and the super-acceleration can be determined by the maximum peak of the 3rd derivative, which could be related to the fracture and removal of asperities and surface layer [52], and localized contact areas caused by increased abrasion, which correlated with higher fluctuations in the curve [57].

In $P_{1.3}$, acceleration reaches its maximum value among all stages, as determined by the negative zero crossing of the 3rd derivative with respect to the *x*-axis. From this point onward, the acceleration begins to decrease, while the velocity and friction values continue to increase. This could be related to the presence of debris with coarser grains from the asperities of the surface layer on the track, which favours plastic deformation [58]. When the initial CoF is low, abrasive wear mechanisms are usually observed [59]. When friction increases significantly, wear particles, primarily from softer and ductile metals, lead to ploughing [60]. Due to plastic deformation, the debris [58] can crack [61], propagate, and eventually separate, leading to their elongation in

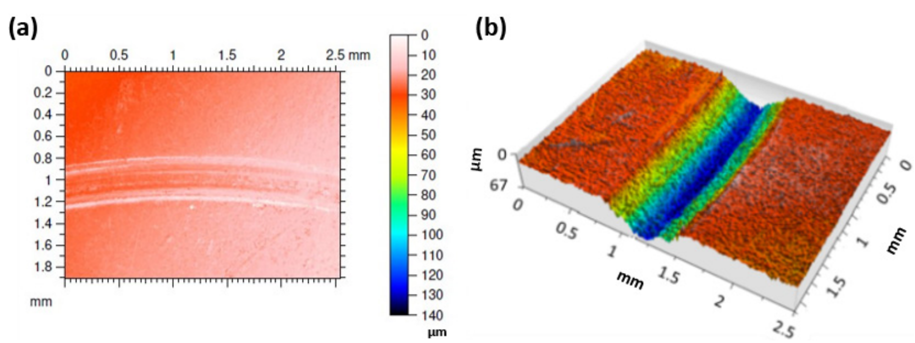

Fig. 9 Topography of as-cast Al80Mg10Si5Cu5 tested BoD at 5 m (50 s): (a) 2D and (b) 3D optical profilometry.

the sliding direction between the two surfaces and thereby decreasing CoF [62]. When plastic deformation occurs, the CoF tends to increase [58] and favours adhesion [50]. The transfer of aluminium from the material to the ball also contributes to the increase in the CoF [63].

At point $P_{1.4}$, the velocity reaches its maximum value among all stages, as identified by the negative zero crossing of the 2nd derivative. From this point onward, deceleration occurs, CoF values continue to increase but at a lower rate, and the amount of debris increases, which in turn amplifies the abrasion [60]. Improved contact could lead to enhanced adhesion mechanisms, with higher initial values and significant oscillations in the coefficient of friction [59].

In point $P_{1.5}$, the super-deceleration reaches its highest value in stage 1, after which the 3rd derivative values start to increase slightly while the CoF shows a minor decrease, as determined by the negative zero crossing of the 4th derivative with respect to the *x*-axis, with the wear track containing fewer debris particles [58].

$P_{1.6}$ corresponds to the first minimum peak of the 2nd derivative in stage 1, as determined by the positive zero crossing of the 3rd derivatives with respect to the *x*-axis. From this point onward, the velocity starts to decrease slightly, indicating a gradual attenuation of the contact dynamics. Only minor plastic deformations are expected, suggesting progressive surface accommodation before the main transition observed at $P_{1.7}$.

At $P_{1.7}$, the 1st derivative approaches zero, while the 2nd derivative reaches a minimum, and the 3rd derivative attains a maximum. This combination indicates a critical transition within stage 1 associated with the formation of a larger real contact area between the ball and the sample, leading to maximum abrasive activity that accelerates the wear rate [11] and promotes the separation of surface asperities from the sample [63]. At this point, the previously accelerated increase in friction diminishes due to severe asperity deformation and intense debris generation.

$P_{1.8}$ is another interesting point to analyse. At this point, the super-acceleration values start to decrease again as the acceleration curve reaches an inflection point, while the velocity values also begin to decrease. This point can be determined by the negative zero crossing of the 3[rd] derivative with respect to the *x*-axis. When the asperities are ploughed and sheared, the debris starts to reorganize or be expelled from the contact, and the contact interface begins to be locally smoothed. As a result, the friction remains high but no longer increases aggressively [54].

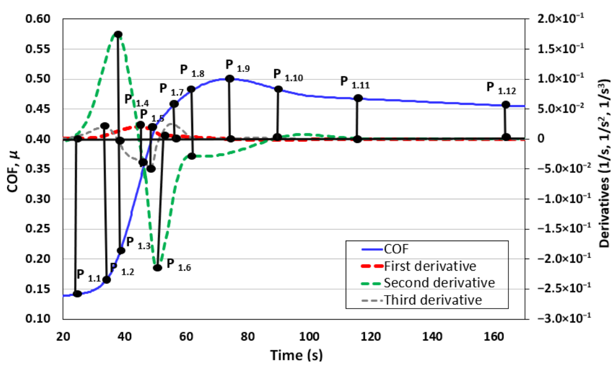

Fig. 10 Detail of stage 1 analysis applying derivatives.

In $P_{1.9}$, the maximum CoF value is reached, but the super-acceleration values are near zero, as determined by the negative zero crossing of the 1[st] derivative with respect to the *x*-axis. At this point, a significant abrasion effect is still observed on the ball [11], while new layers with a composition similar to the AlSiMgCu alloy may adhere to the contact interface, decreasing CoF values [13]. This first peak is common in cases where oxides are present on the surface of the sample, forming a transient protective film [11]. When two friction peaks are observed, the second peak is typically lower than the first one due to the progressive modification of the sliding interfaces caused by prior loading. Conversely, when a second peak is not detected, increased plastic deformation of surface asperities reduces surface roughness, leading to a pronounced decrease in the quasi-static coefficient of friction [54].

Points $P_{1.10}$ and $P_{1.11}$ mark the end transitions of the running-in stage, where the coefficient of friction temporarily stabilizes, but the system still exhibits dynamic readjustments of the contact surfaces. Such internal transitions within the friction profile have been linked in the tribology literature to evolving contact mechanics and surface interactions rather than to fully stable conditions [64].

Point $P_{1.12}$ matches the final of this first stage and coincides with the transition point $P_{2.1}$ of stage 2. At this point, the velocity and acceleration curves exhibit low and stable values, indicating that the running-in dynamics have significantly attenuated. The determination of this transition is often challenging when based solely on the friction curve, which may explain why some studies define the onset of the second stage at the maximum CoF value [65]. In contrast, the present derivative-based approach defines the end of stage 1 as the point at which the combined low values of the first- and higher-order derivatives indicate a stabilized dynamic behaviour, where the influence of previous transient events is no longer dominant. This condition marks the end of the active running-in stage and the onset of a transitional relaxation stage rather than a fully steady-state condition.

Remarkably, from this point onward, the third-derivative signal exhibits more stable behaviour, suggesting a reduction in high-order dynamic fluctuations. This response is consistent with the progressive formation of tribological layers, such as oxide-rich tribolayers [66] or adhesion layers [11], which may promote cleaner contact conditions and contribute to a gradual reduction

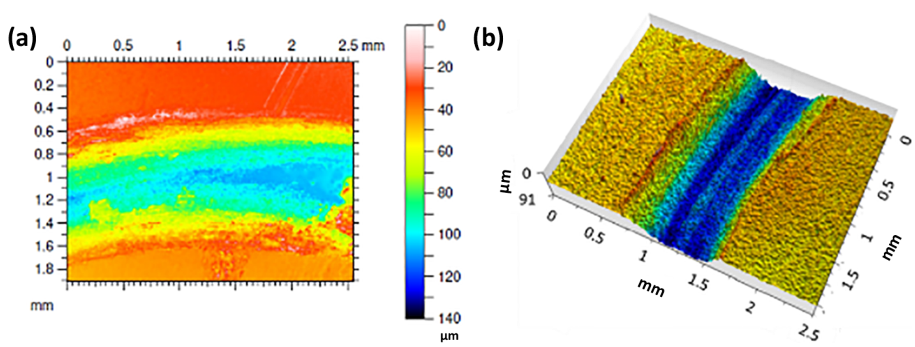

Fig. 11 Topography of Al80Mg10Si5Cu5 tested BoD at 10 m (100 s): (a) 2D and (b) 3D optical profilometry.

Tsinghua University Press | SciOpen

in friction and abrasive wear [37]. The stability of this response may persist until the adhered material layer either stabilizes or is removed, as reported in the literature [11].

During stage 1, the rapid increase in the CoF is consistent with abrasive wear mechanisms such as ploughing and micro-cutting, in which harder asperities and newly generated debris act as micro-cutting edges along the sliding direction. As shown in Fig. 11, the sliding distance range of 5–10 m (50–100 s), corresponding to stage 1, correlates well with the results obtained from 2D and 3D optical surface profilometry analyses. In contrast to the subsequent stages, material removal during this stage is more pronounced, reflecting the severe nature of the running-in process.

It can also be observed that the shape of the track is quite homogeneous, corresponding to the concluding transitions of the running-in stage, where the coefficient of friction temporarily stabilizes, and also, there is a correlation with the corresponding 10 m values in points $P_{1.9}$ to $P_{1.12}$ in the curve.

The debris particles were mainly generated in stage 1 within the 5–10 m (50–100 s) interval. In Fig. 12, the observed particles are characteristic of abrasive micro-ploughing and micro-cutting wear mechanisms [67], which are the primary material removal processes in ductile materials [13, 68, 69]. These particles include stratified structures and grooved features, with micro-ploughing during this stage.

4.4.3 Stage 2

The second stage corresponds to a transitional regime occurring after the maximum CoF peak and before the establishment of the quasi-equilibrium phase. During this stage, strong adhesive junctions formed during the initial loading are progressively sheared and replaced by weaker ones, leading to a decrease in the CoF as plastic deformation becomes dominant and the surface is progressively accommodated [54].

Concurrently, the magnitudes of velocity, acceleration, and super-acceleration decrease, indicating a stabilization of the sliding conditions. The reduction in CoF is further promoted by the increasing role of fine wear debris, which can act as solid lubricants or rollers, partially evolving the contact toward a three-body abrasive regime and favouring tribolayer formation and friction stabilization. The size, morphology, and orientation of the debris play key roles in this process, as fine and active particles can promote tribolayer formation and friction stabilization [70, 71]. When debris particles are oriented perpendicular to the sliding direction, the real contact area is further reduced, contributing to a more stable friction response [11]. In this stage, seven characteristic points can be determined, as shown in Fig. 13.

During stage 2, the system enters a relaxation and accommodation regime in which several internal characteristic points can be identified. Unlike stage 1, these points do not correspond to abrupt changes in the dominant wear mechanism, but rather to progressive adjustments of the contact conditions. The magnitude of the 1st, 2nd, and 3rd derivative signals remains low, while the frequency and amplitude of friction oscillations are progressively reduced, associated with the gradual removal and reorganization of debris, as well as with the growth of an adhered tribolayer on the ball and/or the wear track, which promotes smoother sliding conditions and a gradual decrease in the coefficient of friction [13, 72]. Previous studies have shown that the transition from running-in to stable friction regimes is governed by the formation of aluminium transfer layers on the counterbody surface [73].

The point $P_{2.1}$ corresponds to the start of stage 2, as determined by the positive zero crossing of the 2nd with respect to the zero axis. From this point onward, deceleration reaches its highest value during stage 2, and rotational velocity increases due to the reduced force exerted. The track cleaning process begins.

The intermediate points identified within stage 2 ($P_{2.2}$–$P_{2.6}$) correspond to the moments of progressive relaxation and surface accommodation, rather than to abrupt changes in the dominant wear mechanism.

In $P_{2.2}$, the values for the 3rd derivative reach a local maximum value; while the 1st derivative exhibits its last noticeable oscillation, corresponding to a local minimum, indicating the final transient dynamic adjustment at the onset of stage 2, with a rapid initial reorganization and removal of wear debris [74], resulting in fewer particles on the wear track. The sliding conditions become progressively smoother, facilitating easier motion and contributing to the relaxation of the friction response [64].

At $P_{2.3}$, the 2nd derivative reaches a local maximum, while the 3rd derivative values decrease toward quasi-zero levels, indicating a transient increase in curvature followed by dynamic attenuation. Physically, this reflects progressive debris removal and reorganization, leading to fewer obstacles along the wear track and smoother sliding conditions.

Following point $P_{2.4}$, points $P_{2.5}$ and $P_{2.6}$ present very similar derivative signatures and friction trends, indicating that they belong to the same advanced relaxation regime. In this interval, the CoF continues to decrease gradually, while the velocity and higher-order derivative values remain low and stable. The presence of debris with spherical and cylindrical morphologies can promote a reduction in the CoF by acting as rollers or solid lubricants at the interface under dry sliding conditions [55, 69].

In addition, the progressive reduction in the frequency and amplitude of friction oscillations suggests a decrease in plastic deformation and adhesive interactions [57], which can be associated with the growth of an adhered tribolayer on the ball

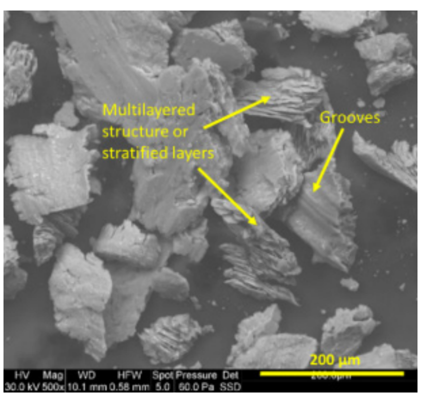

Fig. 12 Morphology of debris caused between 5 and 10 m (50–100 s).

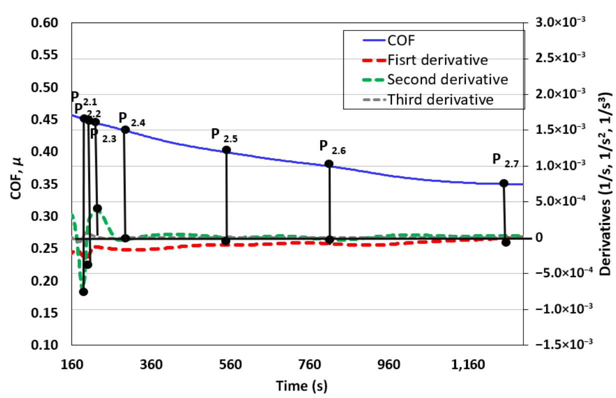

Fig. 13 Detail of friction and derivative curves in stage 2.

and/or the wear track as a result of continued material removal during this stage [13].

Finally, point $P_{2.7}$ is identified by the negative zero crossing of the 2nd derivative with respect to the zero axis, while the 1st derivative reaches a local positive maximum and subsequently starts to decrease. This combined behaviour indicates a change in curvature and the attenuation of the recovery trend, signalling that the relaxation process has concluded, and a new friction regime is being established. This interpretation is consistent with previous studies reporting that running-in and the transition toward more stable sliding conditions are inherently transient and non-stationary processes, which cannot be fully characterized by a single CoF value alone [75].

Figure 14 shows the surface topography corresponding to a sliding distance range of 10–100 m (100–1,000 s), which falls within the near start of stage 2.

The end of stage 1 exhibits fewer abrasion grooves and a reduction in severe ploughing features. However, the surface also presents more pronounced ball indentation marks and localized wear in specific areas, with abrasive mechanisms progressively attenuated during stage 2. These observations are consistent with the relaxation and accommodation regime in stage 2, where the contact becomes smoother, although local stress concentrations can lead to isolated wear events [75].

4.4.4 Stage 3

Stage 3 begins at point $P_{3.1,}$ where the coefficient of friction reaches a quasi-stationary regime characterized by a near-zero slope and consistently lower values of the 1st and higher-order derivatives. This point marks the establishment of a stable sliding response [72], in which transient dynamic effects are no longer dominant. In this stage, the velocity and acceleration signals exhibit their lowest magnitudes, while the super-acceleration remains close to zero, indicating a strongly damped system response. From this point onward, wear is governed by stable and sustained mechanisms, primarily abrasive micro-cutting combined with plastic deformation of surface asperities. These mechanisms operate under relatively constant contact conditions, leading to gradual material removal without significant changes in the friction response. Such a stable friction regime is particularly relevant for applications such as brakes and clutches, where a constant coefficient of friction is required to avoid undesirable vibrations or jerky motion [76]. Three characteristic points can be identified within stage 3. As shown in Fig. 15, abrasive micro-cutting is still observed during the transitional interval preceding $P_{3.2}$, whereas from $P_{3.2}$ onward the wear process is dominated by stable abrasion combined with plastic deformation under quasi-stationary sliding conditions.

Point $P_{3.1}$ marks the onset of stage 3, corresponding to the establishment of a quasi-stationary sliding regime, and is determined by the negative zero crossing of the 2nd derivative with respect to the *x*-axis. At this point, the CoF exhibits a near-zero slope, and all derivative signals remain low and stable, indicating the absence of transient dynamic effects.

Point $P_{3.2}$ corresponds to the consolidation of stage 3, associated with the establishment of a quasi-stationary sliding regime. This point is identified by the negative zero crossing of the 1st and 2nd derivatives with respect to the *x*-axis, followed by low and stable derivative values. At this stage, the CoF exhibits a near-zero slope, indicating the complete attenuation of residual transient dynamic effects. This behaviour suggests that plastic deformation becomes a sustained wear contribution under stable contact conditions, associated with an increased real contact area and possible mild oxidative or microstructural strengthening effects [58]. From $P_{3.2}$ onward, the contact conditions become repetitive and well established [15], allowing the dominant wear mechanisms to operate in a sustained manner under stable sliding conditions.

The final characteristic point is $P_{3.3}$. At this point, both the 1st and 2nd derivative values become slightly negative, although their magnitudes remain very low. This behaviour indicates a minor attenuation of the friction response within the established sliding regime. Consequently, the coefficient of friction becomes increasingly constant, confirming the persistence of stable and repetitive contact conditions characteristic of stage 3.

Figure 16 shows the surface topography corresponding to a sliding distance range of 100–500 m (1,000–5,000 s), which falls within stage 3. The surface profilometry analyses reveal a wear track characterized by a greater penetration depth of the ball into the surface, together with more pronounced abrasion grooves between adjacent indentation regions. This topographical response indicates that, under quasi-stationary sliding conditions, wear is dominated by the combined action of abrasion and plastic deformation. The increased ball indentation reflects a larger real contact area and sustained plastic flow, while the presence of localized abrasion grooves suggests continuous material removal between successive contact zones. These observations are fully consistent with the stable friction regime identified from the friction curve and its derivatives during stage 3.

It can be observed that in the regions of $P_{3.2}$ and $P_{3.3}$, corresponding to the analysed topography, there is a quasi-stationary regime, with steady modifications in the wear track.

During the friction test, different wear mechanisms exhibiting both cyclic and continuous behaviour were identified. The analysis of the 1st, 2nd, and 3rd derivatives of the CoF allowed the characterization of the dynamic state of the contact and the identification of transition and stabilization regimes along the friction curve. Periods characterized by high derivative magnitudes and pronounced fluctuations of the CoF were

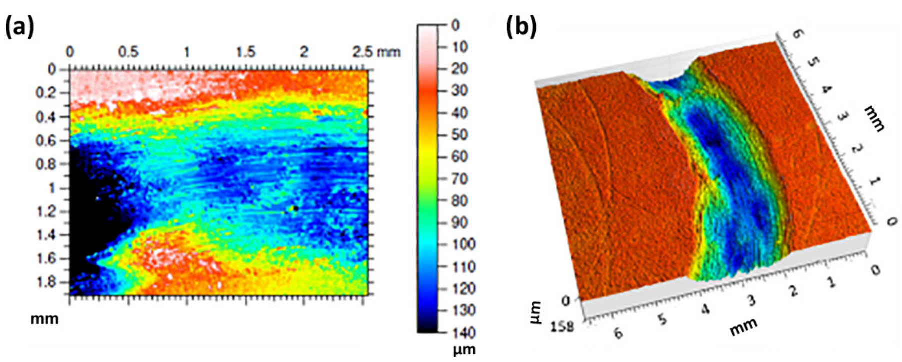

Fig. 14 Topography of Al80Mg10Si5Cu5 tested BoD at 100 m (1,000 s): (a) 2D and (b) 3D optical profilometry.

清華大学出版社 Tsinghua University Press | SciOpen

associated with severe abrasive interactions and rapid surface evolution, particularly during the early stages of the test. In contrast, stages where the derivative values progressively decreased and remained close to zero were indicative of stabilized contact conditions, under which abrasion combined with plastic deformation became the dominant sustained wear mechanisms. Furthermore, prolonged intervals of low derivative activity and nearly constant CoF values were consistent with the formation and stabilization of tribochemical or tribomechanical surface layers, promoted by thermomechanical and thermochemical interactions at the sliding interface [77–79]. In such quasi-steady or steady sliding regimes, the stabilization of the CoF is commonly linked to the development of transfer layers and/or oxide-rich tribofilms [80, 81], which reduce direct metal-to-counterbody contact and moderate wear. In AlSiMg-based alloys, the presence of Cu [81] and larger spherical silicon particles [82] has been reported to promote the formation of protective oxide layers,

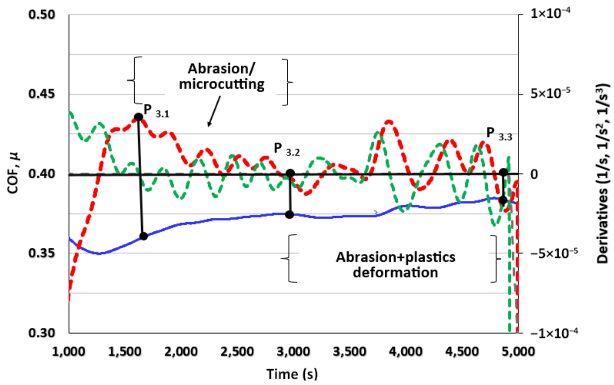

Fig. 15 Detail of friction and derivative curves in stage 3.

contributing to a reduced wear rate [83]. In addition, fine and active wear debris generated during steady sliding may further assist tribolayer formation, reinforcing friction stabilization over time.

Finally, Table 5 summarizes the raw and smoothed CoF values, together with their 1st, 2nd, and 3rd derivatives. Each stage corresponds to a distinct tribological regime, ranging from low-dynamic contact to quasi-stationary wear. Significant differences of more than one order of magnitude are observed between the derivatives, highlighting their sensitivity to changes in the tribological behaviour, their capability to capture changes in the evolution, and stability of the frictional response.

4.5 Use of derivative-based analysis on stage area percentage determination

Figure 17 compares the stage segmentation obtained from the smoothed CoF curve using a conventional qualitative (visual) approach with that obtained by applying the derivative-based methodology. Visual inspection assigned only ~1% of the total area under the CoF curve to the running-in stage (stage 1), whereas the derivative-based approach increased this contribution to ~4%. As a result, the relative contributions of stage 2 and stage 3 are redistributed (from 25% to 29% and from 74% to 66%, respectively).

The running-in stage involves a rapid friction and surface evolution that may not be evident from the CoF trend alone. The use of 1st, 2nd, and 3rd order derivatives enables a more objective identification of this highly active wear stage, which is particularly relevant given that the area under the friction curve in the early stages has been correlated with specific wear rate. Since stage 1 is associated with severe abrasive interactions, visual segmentation

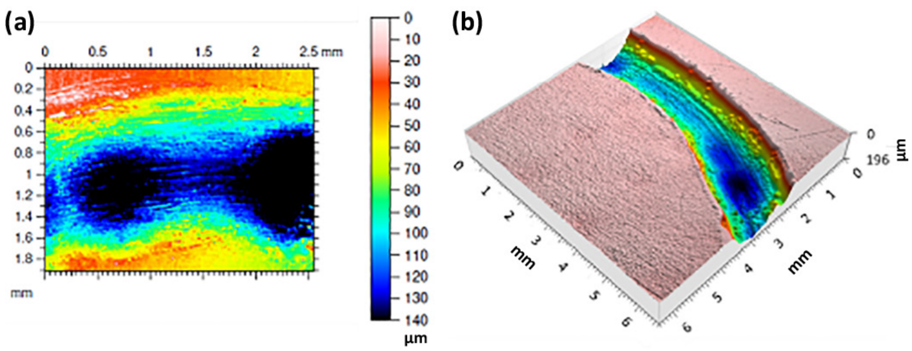

Fig. 16 Topography of Al80Mg10Si5Cu5 tested BoD at 500 m (5,000 s): (a) 2D and (b) 3D optical profilometry.

Table 5 Mean, maximum, and deviation of CoF and its derivatives across different tribological stages

Stage	Raw COF	Smooth COF	d(COF)/dt	d^2(COF)/dt^2	d^3(COF)/dt^3
			Stage 0		
Mean value	1.39×10^{-1}	1.32×10^{-1}	7.60×10^{-4}	1.06×10^{-5}	-3.98×10^{-6}
Standard deviation	7.72×10^{-3}	2.56×10^{-6}	8.06×10^{-6}	3.54×10^{-7}	3.98×10^{-7}
			Stage 1		
Mean value	3.51×10^{-1}	3.25×10^{-1}	6.74×10^{-3}	1.28×10^{-4}	-2.68×10^{-5}
Standard deviation	2.68×10^{-2}	0.00	1.01×10^{-4}	7.66×10^{-6}	4.53×10^{-7}
			Stage 2		
Mean value	4.01×10^{-1}	4.08×10^{-1}	-1.70×10^{-4}	4.53×10^{-6}	6.55×10^{-8}
Standard deviation	6.10×10^{-3}	0.00	6.31×10^{-6}	1.91×10^{-7}	7.74×10^{-9}
			Stage 3		
Mean value	3.79×10^{-1}	3.73×10^{-1}	8.60×10^{-6}	-5.23×10^{-9}	-8.87×10^{-12}
Standard deviation	5.49×10^{-3}	3.89×10^{-5}	6.88×10^{-8}	6.82×10^{-10}	5.45×10^{-12}

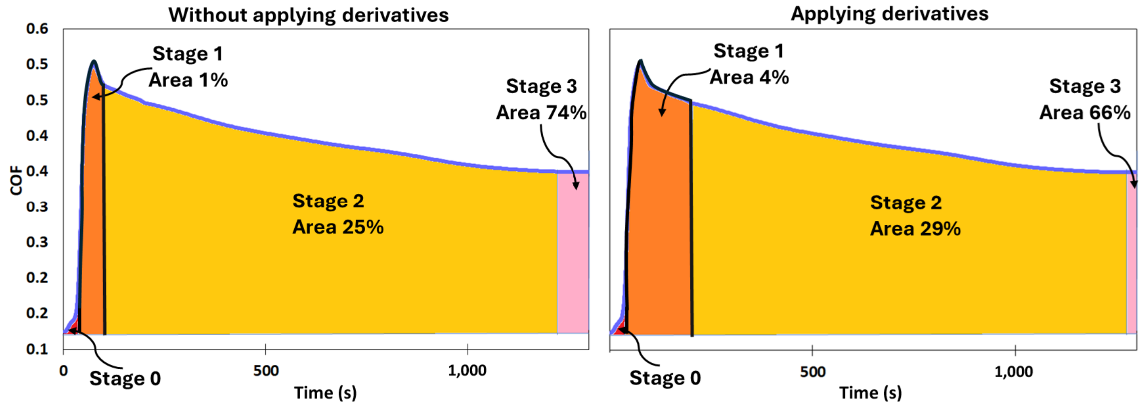

Fig. 17 Comparison of stage segmentation methods.

may underestimate its duration, leading to an incomplete assessment of wear severity.

5 Conclusions

This work has demonstrated the utility of a derivative-based analysis of the CoF for the identification and interpretation of wear stages during BoD tests performed on an Al80Mg10Si5Cu5 HPDC alloy sliding against an Al_2O_3 counterbody. By combining the use of the CoF derivatives with surface and subsurface analyses, the following conclusions can be drawn:

(1) The correlation between the derivative-based identification of stage boundaries and the observed wear surface morphology confirmed that the proposed methodology could enable objective determination of the duration and sequence of the different friction and wear stages.

(2) The selection of an appropriate filtering strategy is essential for reliable results. The centred moving average filter provided a suitable balance between signal smoothing and preservation of curve morphology, ensuring stable and consistent stage identification.

(3) The application of higher-order derivatives allows the detection of characteristic points that are not evident from the CoF curve alone, enabling a more accurate identification of the onset and termination of highly dynamic and transitional wear stages, and could be a useful tool for the control and anticipation of changes in wear mechanisms and the automation of wear control systems.

(4) The transient stage was shown not to coincide with the maximum CoF value but to occur shortly afterwards, being associated with a pronounced minimum in the second derivative. This feature reflects a strong attenuation of friction dynamics and marks the transition from the highly dynamic regime to a more stabilized one.

(5) Although the absolute values of friction and wear depend on the tribological pair and test conditions, the proposed derivative-based methodology could generally apply to other materials and sliding configurations for the identification and monitoring of wear stages.

Acknowledgements

This work has been partially funded by the Basque Government through the ELKARTEK KK-2025/00041 (DESGAS+), KK-2024/00021 (H2MAT+), and by the Department of Research and Universities of the Basque Government IT1542-22.

Author contributions

Ester Villanueva: conceptualization, methodology, formal analysis and investigation, writing - original draft preparation. Iban Vicario: conceptualization, methodology, formal analysis and investigation, writing - review and editing, funding acquisition, supervision. Joseba Albizuri: conceptualization, methodology, formal analysis and investigation, writing - review and editing, funding acquisition, supervision. Raúl Cosgaya: methodology, writing - original draft preparation, resources. Teresa Guraya: writing - review and editing, resources. Iñaki Hurtado: writing - original draft preparation, resources.

Declaration of competing interest

The authors have no competing interests to declare that are relevant to the content of this article.

References

[1] Davim J P. *Tribology for Engineers: A Practical Guide*. Cambridge (UK): Woodhead publishing, 2011.

[2] Davim J P. *Wear of Advanced Materials*. London (UK): Wiley-ISTE, 2013.

[3] Vencl A, Vaxevanidis N M, Kandeva M. A bibliometric analysis of scientific research on tribology of composites in Southeastern Europe. *IOP Conf Ser—Mater Sci* **724**(1): 012012 (2020)

[4] Zhang T, Jiang F, Yan L, Jiang Z Y, Xu X P. A novel ultrahigh-speed ball-on-disc tribometer. *Tribol Int* **157**: 106901 (2021)

[5] Iliev C. On the wear measurement and calculation in ball on disc test. In: Proceedings of World Tribology Congress III, 2005: 49–50.

[6] Jimbert P, Iturrondobeitia M, Ibarretxe J, Fernandez-Martinez R. Pin on disk against ball on disk for the evaluation of wear improvement on cryo-treated metal cutting shears. *AIP Conf Proc* **1653**: 020048 (2015)

[7] Dzierwa A, Pawlus P, Zelasko W. Comparison of tribological behaviors of one-process and two-process steel surfaces in ball-on-disc tests. *P I Mech Eng J—J Eng* **228**(10): 1195–1210 (2014)

[8] Torkashvand K, Selpol V K, Gupta M, Joshi S. Influence of test conditions on sliding wear performance of high velocity air fuel-sprayed WC–CoCr coatings. *Materials* **14**(11): 3074 (2021)

[9] García-León R A, Martínez-Trinidad J, Zepeda-Bautista R, Campos-Silva I, Guevara-Morales A, Martínez-Londoño J, Barbosa-Saldaña J. Dry sliding wear test on borided AISI 316L stainless steel under ball-on-flat configuration: A statistical analysis. *Tribol Int* **157**: 106885 (2021)

[10] Krbata M, Eckert M, Majerik J, Barenyi I. Wear behaviour of high strength tool steel 90MnCrV8 in contact with Si_3N_4. *Metals* **10**(6): 756 (2020)

[11] Ba E C T, Dumont M R, Martins P S, Drumond R M, Martins da Cruz M P, Vieira V F. Investigation of the effects of skewness R_{sk} and kurtosis R_{ku} on tribological behavior in a pin-on-disc test of surfaces machined by conventional milling and turning processes. *Mat Res* **24**(2): e20200435 (2021)

[12] Stembalski M, Preś P, Skoczyński W. Determination of the friction coefficient as a function of sliding speed and normal pressure for steel C45 and steel 40HM. *Arch Civ Mech Eng* **13**(4): 444–448 (2013)

[13] Salguero J, Vazquez-Martinez J M, Del Sol I, Batista M. Application of pin-on-disc techniques for the study of tribological interferences in the dry machining of A92024-T3 (Al–Cu) alloys. *Materials* **11**(7): 1236 (2018)

[14] Tocci M, Pola A, Girelli L, Lollio F, Montesano L, Gelfi M. Wear and cavitation erosion resistance of an AlMgSc alloy produced by DMLS. *Metals* **9**(3): 308 (2019)

[15] Nedeloni M D, Birtărescu E, Nedeloni L, Ene T, Băra A, Clavac B. Cavitation erosion and dry sliding wear research on X5CrNi18-10 austenitic stainless steel. *IOP Conf Ser—Mater Sci* **416**: 012028 (2018)

[16] Raghavendra C R. Analysis of tribological behavior, pin temperature, and surface roughness of a brake pad material with nano coating. *Tribol Int* **197**: 109727 (2024)

[17] Devenport T M, Griffin J M, Rolfe B F, Pereira M P. Friction and wear in stages of galling for sheet metal forming applications. *Lubricants* **11**(7): 288 (2023)

[18] Villanueva E, Albizuri J, Caballero P, Guraya T, Vicario I. Prediction of wear rate by a new direct method using the friction coefficient curve. *J Manuf Mater Proc* **9**(1): 6 (2025)

[19] Domínguez García S, Béjar Gómez L, Maya Yescas R, Lara Romero J, Castro Cedeño B, Espinosa Medina M A. Friction coefficient dynamics of tribological coatings from engine lubricants: Analysis and interpretation. *Coatings* **13**(10): 1753 (2023)

[20] Totten G E. *Friction, Lubrication, and Wear Technology*. Ohio (USA): ASM International, 2017.

[21] Islam M A, Farhat Z. Wear of A380M aluminum alloy under reciprocating load. *J Mater Eng Perform* **19**(8): 1208–1213 (2010)

[22] Suh N P. The delamination theory of wear. *Wear* **25**(1): 111–124 (1973)

[23] Mezlini S, Kapsa P, Henon C, Guillemenet J. Abrasion of aluminium alloy: Effect of subsurface hardness and scratch interaction simulation. *Wear* **257**(9–10): 892–900 (2004)

[24] Hokkirigawa K, Kato K. An experimental and theoretical investigation of ploughing, cutting and wedge formation during abrasive wear. *Tribol Int* **21**(1): 51–57 (1988)

[25] Davim J P. Tribology: A bibliometric analysis. *Int J Surf Sci Eng* **19**(1): 1–3 (2025)

[26] Deleanu L, Georgescu C, Sucio C. A comparison between 2D and 3D surface parameters for evaluating the quality of surfaces. *Ann "Dunărea De Jos" Univ Galați—V* **1**: 5–12 (2012)

[27] Otarawanna S, Gourlay C M, Laukli H I, Dahle A K. Formation of the surface layer in hypoeutectic Al-alloy high-pressure die castings. *Mater Chem Phys* **130**(1–2): 251–258 (2011)

[28] Otarawanna S, Denmud N, Vetayanugul B, Phongphisutthinan C. Microstructural characteristics of the surface layer in high-pressure die castings. *Int J Cast Metal Res* **28**(6): 356–364 (2015)

[29] Davim J P. *Statistical and Computational Techniques in Manufacturing*. Heidelberg (Germany): Springer, 2012.

[30] Gómez I V, Viteri E V, Montero J, Djurdjevic M, Huber G. The determination of dendrite coherency point characteristics using three new methods for aluminum alloys. *Appl Sci* **8**(8): 1236 (2018)

[31] Villanueva E, Vicario I, Sánchez J M, Crespo I. Determination of solidification of rigidity point temperature using a new method. *Appl Sci* **10**(7): 2472 (2020)

[32] Sparkman D. Micro event analysis of cooling curves. Meltlab Systems, 2019. Available at https://meltlab.com/wp-content/uploads/2020/07/Micro-Event-Analysis-of-Cooling-Curves.pdf

[33] Sparkman D A. Quantifying an arrest in thermal analysis. Meltlab Systems, 2010. Available at http://www.meltlab.com/hottopics/august2010quantifiingarrests.pdf

[34] Ciaurri D E, Isebor O J, Durlofsky L J. Application of derivative-free methodologies to generally constrained oil production optimization problems. *Procedia Comput Sci* **1**(1): 1301–1310 (2010)

[35] Awadalla M, Chaouk A, Jneid M, Abuasbeh K, Alahmadi J. Processing the controllability of control systems with distinct fractional derivatives via Kalman filter and gramian matrix. *Fractal Fract* **8**(1): 52 (2024)

[36] Villanueva E, Vicario I, Crespo I, Guraya T, Hurtado I, Albizuri J. A new $Al_{80}Mg_{10}Si_5Cu_5$ multicomponent aluminium alloy: Microstructure, mechanical, and physical properties. *J Mater Res Technol* **37**: 2418–2433 (2025)

[37] Villanueva E, Vicario I, Albizuri J, Arruebarrena G, Guraya T. Wear properties of a new $Al_{80}Mg_{10}Si_5Cu_5$ multicomponent alloy. *Wear* **558–559**: 205585 (2024)

[38] Smith S W. *The Scientist and Engineer's Guide to Digital Signal Processing*. Poway (USA): California Technical Publishing, 1999.

[39] Lyons R G. *Understanding Digital Signal Processing*. London (UK): Pearson, 2011.

[40] Thompson M T. Analog low-pass filters. In: *Intuitive Analog Circuit Design*. Thompson M T, Ed. Amsterdam (the Netherlands): Elsevier, 2014: 531–583.

[41] Darawsheh H Y, Tarczynski A. Comparison between uniform and nonuniform interpolation techniques for digital alias-free FIR filtering. In: Proceedings of the International Conference on Digital Image & Signal Processing, 2019: 978–979.

[42] Crenna F, Rossi B G, Berardengo M. Filtering biomechanical signals in movement analysis. *Sensors* **21**(13): 4580 (2021)

[43] Castañeta H, Nogales J, Zota V. Introducción a la termodinámica con derivadas parciales. *Rev Cs Farm y Bioq* **2**(1): 65–80 (2014) (in Spanish)

[44] Djurdjevic M B, Vicario I, Huber G. Review of thermal analysis applications in aluminium casting plants. *Rev Metal* **50**(1): e004 (2014)

[45] US-ASTM. ASTM G99-05 Standard test method for wear testing with a pin-on-disk apparatus. ASTM, 2010.

[46] Maculotti G, Goti E, Genta G, Mazza L, Galetto M. Uncertainty-based comparison of conventional and surface topography-based methods for wear volume evaluation in pin-on-disc tribological test. *Tribol Int* **165**: 107260 (2022)

[47] Canabarro A, Figueiredo F, Paciornik S, De-Deus G. Two- and three-dimensional profilometer assessments to determine titanium roughness. *Scanning* **31**(4): 174–179 (2009)

[48] Pérez A T, Battez A H, García-Atance G, Viesca J L, González R, Hadfield M. Use of optical profilometry in the ASTM D4172 standard. *Wear* **271**(11–12): 2963–2967 (2011)

[49] Pawlus P, Dzierwa A. Wear analysis of discs and balls on a micro-scale. *Teh Vjesn* **25**: 299–305 (2018)

[50] Stachowiak G W, Batchelor A W. Adhesion and adhesive wear. In: *Engineering Tribology*. Stachowiak G W, Batchelor A W, Eds. Amsterdam (the Netherlands): Elsevier, 1993: 613–635.

[51] Yang X, Zhang Q L, Zheng Y, Liu X C, Politis D, El Fakir O, Wang L L. Investigation of the friction coefficient evolution and lubricant breakdown behaviour of AA7075 aluminium alloy forming processes at elevated temperatures. *Int J Extreme Manuf* **3**(2): 025002 (2021)

[52] Joseph J, Haghdadi N, Shamlaye K, Hodgson P, Barnett M, Fabijanic D. The sliding wear behaviour of CoCrFeMnNi and Al_xCoCrFeNi high entropy alloys at elevated temperatures. *Wear* **428–429**: 32–44 (2019)

[53] Wu J M, Lin S J, Yeh J W, Chen S K, Huang Y S, Chen H C. Adhesive wear behavior of AlxCoCrCuFeNi high-entropy alloys as a function of aluminum content. *Wear* **261**(5–6): 513–519 (2006)

[54] Espinosa H D, Patanella A J, Fischer M. Dynamic friction measurements at sliding velocities representative of high-speed machining processes. *J Tribol—T ASME* **122**(4): 834–848 (2000)

[55] Information on https: //www. tribonet. org/wiki/galling/https://www.tribonet.org/wiki/wear-debris/

[56] Information on https://www.vocabulary.com/dictionary/jerk

[57] Rapoport L, Moshkovich A, Perfilyev V, Lapsker I, Kugler M, Kailer A, Renz A, Hollstein T. High temperature friction behavior of CrV_xN coatings. *Surf Coat Tech* **238**: 207–215 (2014)

[58] Grützmacher P G, Rammacher S, Rathmann D, Motz C, Mücklich F, Suarez S. Interplay between microstructural evolution and tribo-chemistry during dry sliding of metals. *Friction* **7**(6): 637–650 (2019)

[59] Vilaseca M, Molas S, Casellas D. High temperature tribological behaviour of tool steels during sliding against aluminium. *Wear* **272**(1): 105–109 (2011)
[60] Hwang D H, Kim D E, Lee S J. Influence of wear particle interaction in the sliding interface on friction of metals. *Wear* **225–229**: 427–439 (1999)
[61] Waterhouse R B. The role of adhesion and delamination in the fretting wear of metallic materials. *Wear* **45**(3): 355–364 (1977)
[62] Kumar S, Pandey R, Panwar R S, Pandey O P. Effect of particle size on wear of particulate reinforced aluminum alloy composites at elevated temperatures. *J Mater Eng Perform* **22**(11): 3550–3560 (2013)
[63] Domitner J, Silvayeh Z, Sabet A S, Öksüz K I, Pelcastre L, Hardell J. Characterization of wear and friction between tool steel and aluminum alloys in sheet forming at room temperature. *J Manuf Process* **64**: 774–784 (2021)
[64] Blau P J. *Friction Science and Technology from concepts to applications*. Boca Raton (USA): CRC Press, 2008.
[65] Wei Z, Wu Y P, Yang W H, Hong S, Qiao L, Cheng J. Effects of loads on high-temperature wear properties of HVOF sprayed CoCrAlYTa–10%Al_2O_3 and Cr_3C_2–NiCr coatings. *Mater Res Express* **6**(10): 106541 (2019)
[66] De Oliveira M M, Costa H L, Silva W M, De Mello J D B. Effect of iron oxide debris on the reciprocating sliding wear of tool steels. *Wear* **426–427**: 1065–1075 (2019)
[67] Kumar S, Aggarwal A, Jain G. Wear studies of aluminum–silicon alloys. *Int J Res In Mech Eng Tech* **4**(2): 186–189 (2014)
[68] Sharma S, Nanda T R, Pandey O P. Heat treatment T4 and T6 effects on the tribological properties of sillimanite mineral-reinforced LM30 aluminium alloy composites at elevated temperatures. *P I Mech Eng J —J Eng* **236**(5): 946–959 (2022)
[69] Zmitrowicz A. Wear debris: A review of properties and constitutive models. *J Theor App Mech-Pol* **43**(1): 3–35 (2005)
[70] Sharma S, Nanda T, Pandey O P. Investigation of T4 and T6 heat treatment on the wear properties of sillimanite reinforced LM30 aluminium alloy composites. *Wear* **426–427**: 27–36 (2019)
[71] Costa H L, Oliveira Junior M M, de Mello J D B. Effect of debris size on the reciprocating sliding wear of aluminium. *Wear* **376–377**: 1399–1410 (2017)
[72] Páczelt I, Mróz Z. On the analysis of steady-state sliding wear processes. *Tribol Int* **42**(2): 275–283 (2009)
[73] Hu Y, Zheng Y, Politis D J, Masen M A, Cui J, Wang L. Development of an interactive friction model to predict aluminum transfer in a pin-on-disc sliding system. *Tribol Int* **130**: 216–228 (2019)
[74] Sajjad S. Role of wear debris in sliding wear. B. Eng. Thesis. Munich (Germany): Technical University of Munich, 2016.
[75] Khonsari M M, Ghatrehsamani S, Akbarzadeh S. On the running-in nature of metallic tribo-components: A review. *Wear* **474–475**: 203871 (2021)
[76] Information on https://www.roymech.co.uk/Useful_Tables/Drive/Brake_Clutch_mat.html
[77] Hardell J, Hernandez S, Mozgovoy S, Pelcastre L, Courbon C, Prakash B. Effect of oxide layers and near surface transformations on friction and wear during tool steel and boron steel interaction at high temperatures. *Wear* **330–331**: 223–229 (2015)
[78] Javaheri V, Porter D, Kuokkala V T. Slurry erosion of steel—Review of tests, mechanisms and materials. *Wear* **408–409**: 248–273 (2018)
[79] Raghavendra C R, Basavarajappa S, Sogalad I. Sliding wear behaviour of Ni–α-Al_2O_3 nano composite coating at elevated temperatures. *Colloid Interfac Sci* **27**: 18–25 (2018)
[80] Kim H J, Windl W, Rigney D. Structure and chemical analysis of aluminum wear debris: Experiments and *ab initio* simulations. *Acta Mater* **55**(19): 6489–6498 (2007)
[81] Prabhudev M S, Auradi V, Venkateswarlu K, Siddalingswamy N H, Kori S A. Influence of Cu addition on dry sliding wear behaviour of A356 alloy. *Procedia Eng* **97**: 1361–1367 (2014)
[82] Schütte M R, Ehrich J, Linsler D, Hanke S. Effects of microstructure modification by friction surfacing on wear behavior of Al alloys with different Si contents. *Materials* **15**(5): 1641 (2022)
[83] Rahaman M L, Zhang L C. An investigation into the friction and wear mechanisms of aluminium high silicon alloy under contact sliding. *Wear* **376–377**: 940–946 (2017)

Ester Villanueva Viteri is a technical engineer in general chemistry specializing in metallurgical (2012), and earned her master degree in advanced materials engineering (2015–2017) and recently her Ph.D. degree in the Department of Mechanical Engineering, also at the University of the Basque Country (UPV/EHU). Since 2014, she has been a researcher at TECNALIA Research & Innovation, working in the foundry and metallurgy area. Her research expertise spans the development of innovative metallic alloys, process and treatment optimization, materials recovery and regeneration, and the application of advanced analytical techniques. Also, her expertise includes the study of friction and wear properties (tribology), fatigue behaviour, and fracture mechanics. She has participated in over 360 projects, including European programmes, Basque Government initiatives, and direct contracts with clients. She has presented her work at prominent conferences, including the National Materials Conference (CNMAT 2022 and CNMAT 2024), EUROCORR 2023, and EUROMAT 2025. Dr. Villanueva Viteri's contributions reflect her dedication to advancing materials science and industrial applications.